

# Anisotropic 2D Larkin-Imry-Ma state in polar distorted ABM phase of $^3\text{He}$ in "nematically ordered" aerogel

R. Sh. Askhadullin<sup>+</sup>, V. V. Dmitriev<sup>1)</sup>, P. N. Martynov<sup>+</sup>, A. A. Osipov<sup>+</sup>, A. A. Senin, A. N. Yudin

*P. L. Kapitza Institute for Physical Problems of RAS, 2 Kosygina str., 119334 Moscow, Russia*

<sup>+</sup> *A. I. Leypunsky Institute for Physics and Power Engineering, Obninsk, Kaluga region, Russia*

20 October 2014

We present results of experiments in superfluid phases of  $^3\text{He}$  confined in aerogel which strands are nearly parallel to one another. High temperature superfluid phases of  $^3\text{He}$  in this aerogel (ESP1 and ESP2) are chiral phases and have polar distorted ABM order parameter which orbital part forms 2D Larkin-Imry-Ma state. We demonstrate that this state can be anisotropic if the aerogel is squeezed in direction transverse to the strands. Values of this anisotropy in ESP1 and ESP2 phases are different, what leads to different NMR properties.

PACS: 67.57.Pq, 67.57.Lm

## 1. INTRODUCTION

A so-called "nematically ordered" (N-) aerogel differs from standard silica aerogels by a high value of a global anisotropy. This aerogel consists of  $\text{Al}_2\text{O}_3 \cdot \text{H}_2\text{O}$  strands which are nearly parallel to one another [1], i.e. it may be considered as aerogel with infinite stretching anisotropy. Investigations of superfluid  $^3\text{He}$  confined in N-aerogel are especially interesting because according to a theory [2] such a strong anisotropy may make a superfluid polar phase more favorable than Anderson-Brinkman-Morel (ABM) phase which corresponds to A phase of bulk  $^3\text{He}$  and to A-like phase of  $^3\text{He}$  in isotropic or weakly anisotropic silica aerogels [3, 4, 5]. A superfluid phase diagram of  $^3\text{He}$  in N-aerogel is different from the case of  $^3\text{He}$  in silica aerogel with similar porosity [6]. The superfluid transition temperature ( $T_{ca}$ ) is slightly (by 3-6%) suppressed in comparison with the transition temperature ( $T_c$ ) of bulk  $^3\text{He}$ . Depending on prehistory, pressure and temperature, three superfluid phases are observed: two Equal Spin Pairing phases (ESP1 or ESP2) and Low Temperature phase (LTP). The ESP1 phase appears on cooling from the normal state. On further cooling the first order transition into the LTP takes place. Due to inhomogeneities of the aerogel, this transition occurs in a wide temperature range ( $\sim 0.05 T_c$ ). On warming from the LTP the back transition into the ESP phase is observed. At high pressures ( $P \geq 10$  bar) the NMR frequency shift in this phase, called ESP2 phase, is greater than in the ESP1 phase at the same conditions.

The LTP has a polar distorted Balian-Werthamer (BW) order parameter [7]. As for ESP phases,

their NMR properties point out that they both have ABM order parameter with a strong polar distortion [6]. This distortion is larger at low pressures and at higher temperatures. It was also found that the order parameter orbital vector  $\mathbf{l}$  of the distorted ABM phase in N-aerogel is in a spatially inhomogeneous Larkin-Imry-Ma (LIM) state similar to that predicted in [8] and observed in A-like phase of  $^3\text{He}$  in silica aerogel [4, 9]. In N-aerogel we get the two-dimensional LIM state because the aligned strands orient  $\mathbf{l}$  normal to their axis.

In this paper we present results of nuclear magnetic resonance (NMR) studies of liquid  $^3\text{He}$  confined in N-aerogel which was slightly squeezed in direction transverse to the strands. In particular, these experiments allow us to explain the difference between properties of ESP1 and ESP2 phases.

## 2. THEORY

Transverse NMR frequency shift can be found from the following equation [10]:

$$\Delta\omega = -\frac{g}{\chi H} \frac{\partial \bar{U}_D}{\partial \cos \beta}, \quad (1)$$

where  $g$  is the gyromagnetic ratio,  $\chi$  - the spin susceptibility,  $H$  - the external magnetic field,  $\beta$  - the tipping angle of the magnetization and  $\bar{U}_D$  - the density of the dipole energy, averaged over a fast spin precession. For the LIM state the dipole energy should also be averaged over the space (see e.g. [4, 11]). The order parameter of the ABM phase with polar distortion is:

$$A_{jk} = \Delta_0 e^{i\phi} d_j (am_k + ibn_k), \quad (2)$$

<sup>1)</sup>e-mail: dmitriev@kapitza.ras.ru

where  $\Delta_0$  is the gap parameter,  $\mathbf{d}$  is the unit spin vector,  $\mathbf{m}$  and  $\mathbf{n}$  are mutually orthogonal unit vectors in the orbital space and  $a^2 + b^2 = 1$ . For the ABM phase  $a = b$ , for polar distorted ABM phase  $a^2 > b^2$  and for polar phase  $a = 1, b = 0$ . Similarly to pure ABM phase, the distorted ABM phase is a chiral phase and we can introduce the orbital vector  $\mathbf{l} = \mathbf{m} \times \mathbf{n}$  which orientation defines two Weyl points in the momentum space: the energy gap of this phase equals 0 along  $\mathbf{l}$  and equals  $\sqrt{2}a\Delta_0$  and  $\sqrt{2}b\Delta_0$  along  $\mathbf{m}$  and  $\mathbf{n}$ . Note that the polar phase is not chiral and its gap has line of zeroes in the plane normal to  $\mathbf{m}$ . The dipole energy density for the order parameter (2) is:

$$U_D = \frac{6}{5}g_D (a^2(\mathbf{d}\mathbf{m})^2 + b^2(\mathbf{d}\mathbf{n})^2), \quad (3)$$

where  $g_D = g_D(T)$  is the dipole constant. In weak coupling limit  $g_D$  can be expressed in terms of the Leggett frequency of the pure ABM phase  $\Omega_A$  [12]:

$$g_D = \frac{2}{3 - 4a^2b^2} g_D^A = \frac{2}{3 - 4a^2b^2} \left( \frac{5}{6} \frac{\chi}{g^2} \Omega_A^2 \right), \quad (4)$$

where  $g_D^A$  is the dipole constant of the ABM phase. Strong coupling corrections to (4) do not exceed  $\pm 5\%$  [13], therefore we do not consider them below.

Following [11, 14], we use two coordinate frames: an orbital frame  $(\hat{\xi}, \hat{\eta}, \hat{\zeta})$  bound to the aerogel sample and a spin frame  $(\hat{x}, \hat{y}, \hat{z})$ . We choose  $\mathbf{H} = H\hat{z}$  and fix  $\hat{\zeta}$ -axis along aerogel strands. Then strands of N-aerogel orient  $\mathbf{m} \parallel \hat{\zeta}$  and  $\mathbf{l} \perp \hat{\zeta}$  [2]. In the isotropic 2D LIM state vectors  $\mathbf{l}$  and  $\mathbf{n}$  are randomly distributed in  $\hat{\xi} - \hat{\eta}$  plane and  $\langle l_\xi^2 \rangle = \langle l_\eta^2 \rangle = \langle n_\xi^2 \rangle = \langle n_\eta^2 \rangle = \frac{1}{2}$ , where angle brackets mean the space averaging. We introduce the angle  $\lambda = \lambda(\mathbf{r})$  which defines the orientation of specific  $\mathbf{l}$  and the corresponding  $\mathbf{n}$ :  $l_\xi = -n_\eta = \cos \lambda$  and  $l_\eta = n_\xi = \sin \lambda$ . For uniaxially anisotropic in  $\hat{\xi} - \hat{\eta}$  plane 2D LIM state we fix the  $\hat{\xi}$ -axis along the direction corresponding to the maximum value of  $\langle l_\xi^2 \rangle$ .

Consequently  $1 > \langle l_\xi^2 \rangle > \frac{1}{2} > \langle l_\eta^2 \rangle$  and we assume that the distribution of  $l_\xi = l_\xi(\lambda)$  is symmetric.

An orientation of  $\mathbf{H}$  with respect to the aerogel (Fig.1) is described by angles of rotation of the orbital frame:  $\mu$  (rotation around  $\hat{\xi}$ ) and  $\varphi$  (rotation around  $\hat{\zeta}$ ). Then we get:

$$\begin{aligned} m_x &= 0, \quad m_y = -\sin \mu, \quad m_z = \cos \mu, \\ n_x &= \sin(\varphi + \lambda), \quad n_y = -\cos \mu \cos(\varphi + \lambda), \\ n_z &= -\sin \mu \cos(\varphi + \lambda). \end{aligned} \quad (5)$$

Motions of  $\mathbf{d}$  in the spin frame are described by Euler angles  $(\alpha, \beta, \gamma)$ , where  $\alpha$  corresponds to the phase of

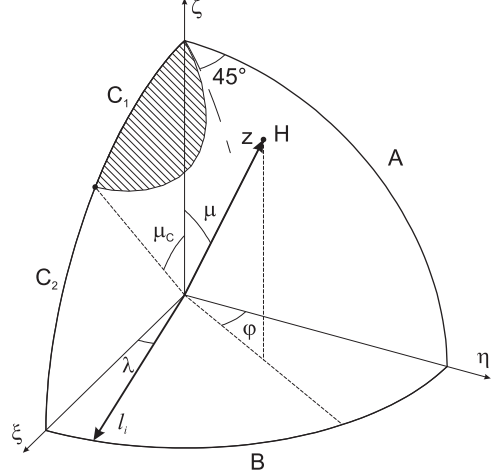


Fig.1. Orientation of  $\mathbf{H}$  with respect to N-aerogel axes.

spin precession and  $\beta$  is the tipping angle. After an averaging over the fast spin precession we obtain:

$$\begin{aligned} \bar{d}_x^2 &= \frac{1}{4} \langle \cos^2 \Phi \rangle (1 + \cos \beta)^2 + \frac{1}{8} (1 - \cos \beta)^2, \\ \bar{d}_y^2 &= \frac{1}{4} \langle \sin^2 \Phi \rangle (1 + \cos \beta)^2 + \frac{1}{8} (1 - \cos \beta)^2, \\ \bar{d}_z^2 &= \frac{1}{2} \sin^2 \beta, \quad \overline{d_x d_z} = \overline{d_y d_z} = 0, \\ \overline{d_x d_y} &= -\frac{1}{8} \langle \sin 2\Phi \rangle (1 + \cos \beta)^2, \end{aligned} \quad (6)$$

where  $\Phi = \alpha + \gamma$  is a slow variable. Then the dipole energy (3) averaged over the space is:

$$\begin{aligned} \bar{U}_D &= \frac{6}{5}g_D \left[ a^2 (\bar{d}_y^2 m_y^2 + \bar{d}_z^2 m_z^2) + \right. \\ &\quad \left. + b^2 (\bar{d}_x^2 \langle n_x^2 \rangle + \bar{d}_y^2 \langle n_y^2 \rangle + \bar{d}_z^2 \langle n_z^2 \rangle + 2\overline{d_x d_y} \langle n_x n_y \rangle) \right], \quad (7) \end{aligned}$$

where  $\langle n_x^2 \rangle = \sin^2 \varphi \langle \cos^2 \lambda \rangle + \cos^2 \varphi \langle \sin^2 \lambda \rangle$ ,  $\langle n_y^2 \rangle = \cos^2 \mu (\cos^2 \varphi \langle \cos^2 \lambda \rangle + \sin^2 \varphi \langle \sin^2 \lambda \rangle)$ ,  $\langle n_z^2 \rangle = \sin^2 \mu (\cos^2 \varphi \langle \cos^2 \lambda \rangle + \sin^2 \varphi \langle \sin^2 \lambda \rangle)$  and  $\langle n_x n_y \rangle = (2 \langle \sin^2 \lambda \rangle - 1) \cos \mu \sin \varphi \cos \varphi$ . The angle  $\Phi$  may be spatially homogeneous (the spin nematic state, SN) or random (the spin glass state, SG) [4]. The SN state is more favorable and corresponds to the homogeneous spatial distribution of  $\mathbf{d}$ , but the SG state may be created e.g. in pulse NMR experiments after an application of large tipping pulses. In the isotropic SG state  $\langle \sin^2 \Phi \rangle = \langle \cos^2 \Phi \rangle = 1/2$  and  $\langle \sin 2\Phi \rangle = 0$  while in the SN state  $\Phi$  is determined by minimization of (7). The result of the minimization is shown in Fig.1 where the shaded area corresponds to orientations of  $\mathbf{H}$  with  $\sin^2 \Phi = 1$  while for other orientations the minimum

of (7) corresponds to  $\sin^2 \Phi = 0$ . The border of the shaded area satisfies to the following condition:

$$b^2(\langle l_\xi^2 \rangle \cos^2 \varphi + \langle l_\eta^2 \rangle \sin^2 \varphi) \cos^2 \mu - \langle l_\xi^2 \rangle \sin^2 \varphi - \langle l_\eta^2 \rangle \cos^2 \varphi + a^2 \sin^2 \mu = 0. \quad (8)$$

In particular, if  $\varphi = 90^\circ$  then  $\sin^2 \Phi = 1$  for  $\mu < \mu_c$  and  $\sin^2 \Phi = 0$  for  $\mu > \mu_c$ , where

$$\sin \mu_c = \frac{b^2(1 - 2\langle l_\eta^2 \rangle)}{1 - b^2 - b^2\langle l_\eta^2 \rangle}. \quad (9)$$

The critical angle  $\mu_c$  corresponds to an orientational transition: in the equilibrium SN state  $\mathbf{d} \perp \hat{\eta}$  for  $\mu < \mu_c$ , while  $\mathbf{d} \parallel \hat{\eta}$  for  $\mu > \mu_c$ .

The NMR frequency shift from the Larmor value can be obtained from (1) and (7):

$$\Delta\omega = \frac{1}{4}K \left[ (a^2 m_y^2 - b^2 \langle n_x^2 \rangle + b^2 \langle n_y^2 \rangle) \times \right. \\ \left. \times (1 - 2\sin^2 \Phi (1 + \cos \beta)) + (4 - 5a^2 m_y^2 - b^2 (7\langle n_x^2 \rangle + 5\langle n_y^2 \rangle)) \cos \beta \right], \quad (10)$$

where

$$K = \frac{2}{3 - 4a^2 b^2} \frac{\Omega_A^2}{\omega}$$

and  $\omega = gH$ . Let consider 4 cases:  $\varphi = 0$ ,  $0 < \mu < 90^\circ$  (the case A);  $\mu = 90^\circ$ ,  $0 < \varphi < 90^\circ$  (B);  $\varphi = 90^\circ$ ,  $0 < \mu < \mu_c$  ( $C_1$ );  $\varphi = 90^\circ$ ,  $\mu_c < \mu < 90^\circ$  ( $C_2$ ). In Fig.1 these orientations of  $\mathbf{H}$  correspond to arcs marked A, B,  $C_1$  and  $C_2$ . Then for the case of continuous wave (CW) NMR ( $\cos \beta \approx 1$ ) we get:

$$\begin{aligned} A : \quad \Delta\omega &= K(D \sin^2 \mu + E \cos^2 \mu), \\ B : \quad \Delta\omega &= KD(1 - 2\sin^2 \varphi), \\ C_1 : \quad \Delta\omega &= KE \cos 2\mu, \\ C_2 : \quad \Delta\omega &= K(E \cos^2 \mu - D), \end{aligned} \quad (11)$$

where  $D = b^2(1 - 2\langle l_\eta^2 \rangle) \geq 0$  and  $E = 1 - b^2 - b^2\langle l_\eta^2 \rangle > 0$ . The dependence of  $\Delta\omega$  on  $\mu$  for  $\varphi = 90^\circ$  is shown in Fig.2. This dependence is fully determined by 2 values of the frequency shift:  $\Delta\omega_\xi = -KD$  ( $\mathbf{H} \parallel \hat{\xi}$ ) and  $\Delta\omega_\zeta = KE$  ( $\mathbf{H} \parallel \hat{\zeta}$ ) so that  $\sin^2 \mu_c = -\Delta\omega_\xi / \Delta\omega_\zeta$ .

In the isotropic 2D LIM state  $\langle l_\eta^2 \rangle = 1/2$  (i.e.  $D = 0$ ) and for  $\mu = 90^\circ$  (the case B)  $\Delta\omega = 0$  in agreement with [6]. If the 2D LIM state is anisotropic and  $\langle l_\eta^2 \rangle < 1/2$ , then for  $\mu = 90^\circ$  the shift equals 0 for  $\varphi = 45^\circ$ . For other values of  $\varphi$  the shift is 0 only for pure polar phase ( $b = 0$ ). In pure ABM phase or in the ABM phase with polar distortion the shift is positive (if  $\varphi < 45^\circ$ ) or negative (if  $\varphi > 45^\circ$ ).

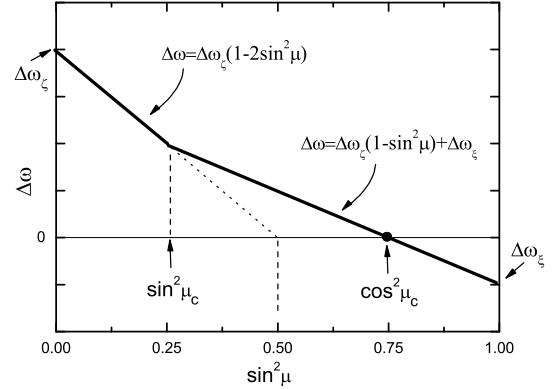


Fig.2. CW NMR frequency shift versus  $\mu$  for  $\varphi = 90^\circ$  as follows from (11).

### 3. EXPERIMENTAL SETUP

The experimental chamber used in the present work is similar to the chamber described in [6]. The chamber has two cells with N-aerogel samples. The samples (named below as 1 and 2) have a form of a cuboid with characteristic sizes of 4 mm. Initially the samples had an overall density  $\sim 30 \text{ mg/cm}^2$  (sample 1) and  $\sim 8 \text{ mg/cm}^2$  (sample 2), but were squeezed by  $\sim 10\%$  and  $\sim 5\%$  correspondingly along the direction transverse to the aerogel strands. In order to match Fig.1 we choose the direction of the squeezing as  $\eta$ -axis, because (see next section) in the anisotropic 2D LIM state of the distorted ABM phase the maximum of  $\langle l_\xi^2 \rangle$  corresponds to this direction of the squeezing.

We were able to rotate  $\mathbf{H}$  by any angle  $\mu$  in  $\hat{\zeta}$ - $\hat{\eta}$  plane (for the sample 1) or in  $\hat{\zeta}$ - $\hat{\xi}$  plane (for the sample 2). Additional gradient coils were used to compensate the external magnetic field inhomogeneity. Experiments were performed in magnetic fields from 104 Oe up to 425 Oe (NMR frequencies were from 340 kHz up to 1.38 MHz) and at pressures from s.v.p. up to 29.3 bar. The necessary temperatures were obtained by a nuclear demagnetization cryostat and were measured by a quartz tuning fork, calibrated by Leggett frequency measurements in bulk  $^3\text{He}$ -B. In order to avoid a paramagnetic signal from surface solid  $^3\text{He}$ , the samples were preplated by  $\sim 2.5$  atomic monolayers of  $^4\text{He}$ .

A superfluid phase diagram of  $^3\text{He}$  in the sample 1 was found to be almost the same as the diagram presented in [6]. For the sample 2 the diagram is slightly different (the superfluid transition temperatures are by 2-3% higher).

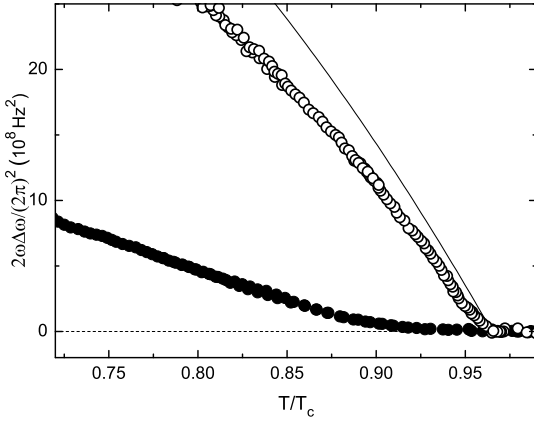


Fig.3. CW NMR frequency shift versus temperature in sample 1. (○) –  $\mathbf{H} \parallel \hat{\xi}$ ; (●) –  $\mathbf{H} \parallel \hat{\eta}$ . Solid line shows  $\Omega_A^2$  rescaled from  $\Omega_{A0}^2$  in accordance with (12) for  $k = 1$ .  $P = 14.2$  bar,  $T_{ca} \approx 0.965 T_c$ .

#### 4. EXPERIMENTS WITH THE SAMPLE 1

Temperature dependencies of CW NMR frequency shifts in the ESP1 phase ( $\Delta\omega_\xi$  and  $\Delta\omega_\eta$ ) for  $\mathbf{H} \parallel \hat{\xi}$  and for  $\mathbf{H} \parallel \hat{\eta}$  are shown in Fig.3. The superfluid transition temperature of  $^3\text{He}$  in this sample at the given pressure (14.2 bar) is  $\sim 0.965 T_c$  as it can be seen from appearance of the NMR shift for  $\mathbf{H} \parallel \hat{\xi}$ . As follows from (11)  $\Delta\omega_\xi = KE$  and  $\Delta\omega_\eta = KD$ . In the experiment, we obtain  $\Delta\omega_\eta = 0$  down to  $\sim 0.93 T_c$  but on further cooling the positive shift appears. It means that for  $T < 0.93 T_c$  both  $b^2$  and  $(1 - 2\langle l_\eta^2 \rangle)$  are nonzero and positive, i.e. we get the distorted ABM phase and the squeezing of the sample along  $\hat{\eta}$  results in preferable orientation of vectors  $\mathbf{l}$  along the  $\hat{\xi}$ -axis.

If value of  $\Omega_A$  is known, then we can find  $b^2$  and  $\langle l_\eta^2 \rangle$  from the measured values of  $\Delta\omega_\xi$  and  $\Delta\omega_\eta$ . The problem is that  $\Omega_A \propto \Delta_0$  is known only for the bulk  $^3\text{He}$  (below we denote this value by  $\Omega_{A0}$ ). The value of  $\Omega_A$  in N-aerogel should be smaller due to the suppression of  $T_c$  and corresponding decrease of the gap. It is known that in silica aerogels the gap suppression is larger than the suppression of  $T_c$  in agreement with the “inhomogeneous isotropic scattering model” [15]. For example, for  $T_{ca} = 0.965 T_c$  the gap and  $\Omega_A$  is suppressed by  $\sim 9\%$  [16]. Another model called the “homogeneous isotropic scattering model” [17] predicts that the gap suppression is proportional to  $T_{ca}/T_c$ . Both these models, however, can not be directly applied to  $^3\text{He}$  in N-aerogel due to its strong anisotropy. Therefore we can only assume that the suppression of  $\Omega_A$  in N-aerogel is proportional to  $T_{ca}/T_c$  or larger, i.e.:

$$\Omega_A(T/T_{ca}) = k \frac{T_{ca}}{T_c} \Omega_{A0}(T/T_c), \quad (12)$$

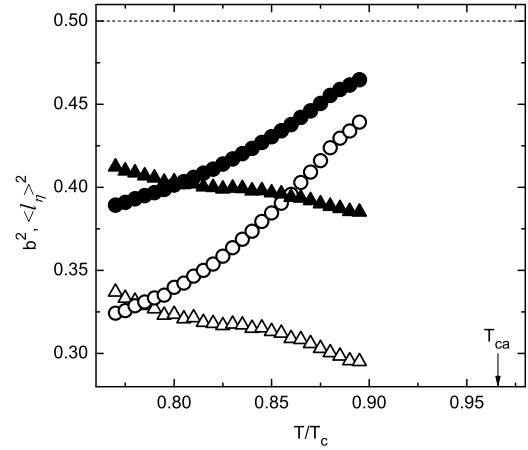


Fig.4.  $\langle l_\eta^2 \rangle$  (circles) and  $b^2$  (triangles) calculated from data in Fig.3 for  $k = 1$  (●, ▲) and for  $k = 0.9$  (○, △).

where  $k \leq 1$ . In Fig.4 we present values of  $b^2$  and  $\langle l_\eta^2 \rangle$  calculated from the data shown in Fig.3 in the assumption that  $k = 1$  or  $k = 0.9$ . It can be seen that  $\langle l_\eta^2 \rangle$  grows on warming and tends to  $1/2$  for both values of  $k$ , while  $b^2$  decreases but can not be extrapolated to 0 for  $T < T_{ca}$ . Thus we conclude that the anisotropy of the 2D LIM state decreases on warming and  $\langle l_\eta^2 \rangle$  becomes equal (or close) to  $1/2$  at  $T > 0.93 T_{ca}$  resulting in  $\Delta\omega_\eta = 0$ . The polar distortion grows on warming but it is unlikely that we get pure polar phase in a reasonably large temperature range near  $T_{ca}$  for these values of  $k$ . At lower pressures ( $P \leq 9$  bar) we have obtained similar dependencies as shown in Figs.2 and 3, but if  $k \leq 0.9$  the value of  $b^2$  can be extrapolated to 0 at  $T < T_{ca}$ , so the existence of the pure polar phase near  $T_{ca}$  can not be excluded, but only if  $k \leq 0.9$ .

#### 5. IDENTIFICATION OF THE ESP2 PHASE (EXPERIMENTS WITH THE SAMPLE 2)

The sample 2 was oriented so that  $\mathbf{H}$  could be rotated in  $\hat{\xi}$ - $\hat{\xi}$  plane. Correspondingly, at low temperatures the anisotropy of the 2D LIM state should result in a negative CW NMR frequency shift for the transverse orientation of the field ( $\mathbf{H} \parallel \hat{\xi}$ ) as follows from  $C_2$  in (11) for  $\mu = 90^\circ$  and  $D > 0$ . Examples of temperature dependencies of the shift in ESP phases for both transverse and parallel orientations of  $\mathbf{H}$  are shown in Fig.5. As it was expected, at low temperatures the shift is negative in both ESP phases for  $\mathbf{H} \parallel \hat{\xi}$ . In this case the absolute value of the shift in the ESP2 phase is larger than in the ESP1 phase.

The difference in the NMR shift in ESP1 and ESP2 phases may be explained either by different values of the

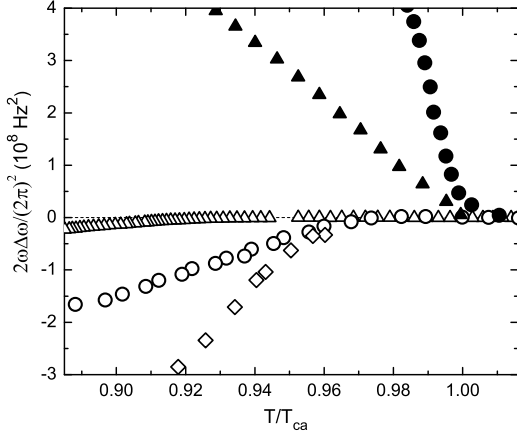


Fig.5. CW NMR frequency shift versus temperature for sample 2. Open symbols –  $\mathbf{H} \parallel \hat{\xi}$ ; filled symbols –  $\mathbf{H} \parallel \hat{\zeta}$ .  $P = 12.3$  bar ( $T_{ca} \approx 0.98 T_c$ ): (●, ○) – ESP1 phase; (◇) – ESP2 phase.  $P = 2.9$  bar ( $T_{ca} \approx 0.95 T_c$ ): (▲, △) – ESP1 phase.

polar distortion (i.e. of  $b^2$ ) or by different values of the anisotropy of the 2D LIM state (i.e. of  $\langle l_\eta^2 \rangle$ ). In both cases the dependence of  $\Delta\omega = \Delta\omega(\mu)$  for the sample 2 should correspond to the dependence shown in Fig.2.

As follows from (9)  $\mu_c > 0$  only if  $\Delta\omega_\xi \neq 0$ . Therefore we have chosen the temperature  $T \approx 0.85 T_{ca}$  where the absolute value of  $\Delta\omega_\xi$  is large enough, but the smeared transition into the LTP just starts. In order to get the ESP2 phase at this temperature the sample was warmed up above the point of full transition to the ESP2 phase ( $\sim 0.93 T_{ca}$ ) and then was cooled down. The obtained dependencies of the CW NMR shift on  $\mu$  are shown in Fig.6 where solid lines are drawn using only the corresponding values of  $\Delta\omega_\xi$  and  $\Delta\omega_\zeta$ . It can be seen that the data are well described by the theory. Further analysis shows that the difference between the ESP phases can not be attributed to the difference of magnitudes of the polar distortion, but can be explained in assumption that the anisotropy of the 2D LIM state in these phases is different. The data in Fig.6 allow to calculate  $b^2$  and  $\langle l_\eta^2 \rangle$  for a given  $k$  in Eq.(12). If  $k = 1$  then  $b^2 = 0.42$  and  $\langle l_\eta^2 \rangle = 0.43$  for the ESP1 phase, and  $b^2 = 0.43$  and  $\langle l_\eta^2 \rangle = 0.33$  for ESP2 phase. For  $k = 0.9$  we get  $b^2 = 0.35$  and  $\langle l_\eta^2 \rangle = 0.39$  for the ESP1 phase, and  $b^2 = 0.36$  and  $\langle l_\eta^2 \rangle = 0.24$  for ESP2 phase. Note that for both values of  $k$  we get nearly equal values of  $b^2$  in both ESP states, while the anisotropy of the 2D LIM state in the ESP2 phase is always greater than in the ESP1 phase. This difference in the anisotropy may be due to the ESP2 phase is formed on warming from the LTP, which order parameter corresponds to a spatially homogeneous polar distorted BW phase. It

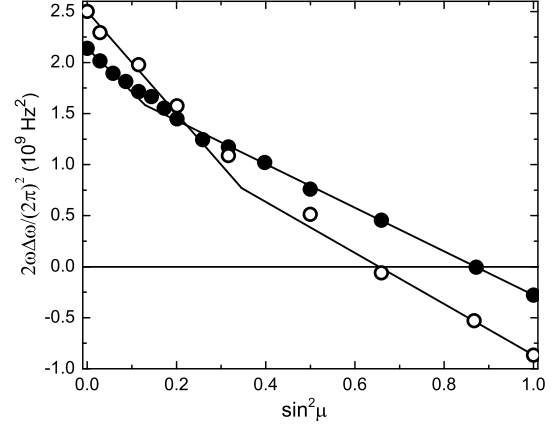


Fig.6. CW NMR frequency shift versus  $\mu$  for sample 2. Solid lines – theoretical dependencies  $C_1$  and  $C_2$  in (11). (●) – ESP1 phase; (○) – ESP2 phase.  $P = 12.3$  bar,  $T \approx 0.85 T_{ca}$ ,  $H = 117$  Oe.

is the first order transition, i.e. the phase boundary moves through the sample providing the orienting effect on  $\mathbf{l}$  and resulting in stabilization of more anisotropic metastable 2D LIM state. Worthy to mark that similar history dependent orientational effect on  $\mathbf{l}$  was observed in ABM phase of  $^3\text{He}$  in silica aerogel [9].

The ESP phases observed in [6] have been obtained in N-aerogel sample which has not been squeezed in transverse direction. In this case the 2D LIM state of the ESP1 phase should be isotropic, but the above mentioned orienting effect should remain resulting in the anisotropic 2D LIM state in the ESP2 phase.

## 6. ORIENTATION OF ORBITAL VECTOR IN N-AEROGEL

The influence of aerogel deformation on a spatial distribution of  $\mathbf{l}$  in ABM-like phase of  $^3\text{He}$  is a complex problem and depends on how  $\mathbf{l}$ -orienting centers are transformed during deformation. Different types of aerogel have different microscopic structures. This can result in a different response of the  $\mathbf{l}$ -field to the deformation. For example, silica aerogels used in [18, 19] orient  $\mathbf{l}$  *along* the axis of stretching and *normal* to the axis of squeezing. On the other hand, N-aerogel (i.e. the infinitely stretched array of cylindric strands) orients  $\mathbf{l}$  normal to the strands, i.e. *normal* to the stretching.

There are three theoretical models describing the influence of the aerogel deformation on  $\mathbf{l}$  [8, 20, 21]. The model [8] considers the aerogel as a system of randomly oriented cylinders and seems to be the most consistent with N-aerogel. The deformation changes an angular distribution of strands and orients the  $\mathbf{l}$ -field.

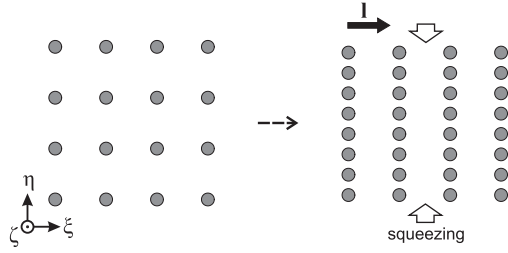


Fig.7. Squeezing of N-aerogel which strands form the 2D square lattice.

The model [8] predicts that  $\mathbf{l}$  tends to align along the axis of squeezing and normal to the axis of stretching. N-aerogel corresponds to the infinite stretching and the model predicts the 2D LIM state in the  $\xi - \eta$  plane in agreement with experiments [6] and with this work.

As it was shown above the squeezing of the N-aerogel in the  $\hat{\xi}-\hat{\eta}$  plane results in preferable orientation of  $\mathbf{l}$  along the direction *normal* to the squeezing direction. At first glance, this disagrees with [8]. However there is no contradiction here: the point is that the squeezing in the  $\hat{\xi}-\hat{\eta}$  plane does not change orientations of the strands, i.e. the orienting effect in frames of the model [8] is absent. However, this type of deformation changes spatial correlations of strands. If these correlations are anisotropic in  $\hat{\xi}-\hat{\eta}$  plane then the orienting force will be along the direction normal to the squeezing. This is illustrated by Fig.7 where the result of the squeezing of N-aerogel is shown for the simplest case of a 2D square lattice of the strands in  $\hat{\xi}-\hat{\eta}$  plane. It can be seen that a strong squeezing results in the formation of “wall-like” structures. These “walls” should orient  $\mathbf{l}$  normal to the surface, i.e. *normal* to the squeezing direction. We think that this effect remains not only for the cubic lattice but also for any locally anisotropic spatial correlations. The similar phenomenon may cause the orienting effect in a 3D lattice of ball-like  $\mathbf{l}$ -orienting centers if their spatial correlations are locally anisotropic. We assume that it may explain orienting effects observed in [18, 19].

## 7. CONCLUSIONS

1. The observed NMR properties of ABM phase with polar distortion of  $^3\text{He}$  in “nematically ordered” aerogel agree with the developed theoretical model. This allows us to explain the difference in NMR properties of the ESP phases: the 2D LIM state of vector  $\mathbf{l}$  in the ESP2 phase is more anisotropic than in the ESP1 phase.

2. We have shown that the squeezing of N-aerogel along the direction normal to the strands results in the anisotropic 2D LIM state in the ESP phases so that the preferable orientation of  $\mathbf{l}$ -field is normal to the

squeezing. The explanation of this effect is suggested. The anisotropy of the 2D LIM state decreases on warming and may disappear below  $T_{ca}$ .

3. The order parameter orientational transition have been observed. The transition occurs when the angle between  $\mathbf{H}$  and the axis of the anisotropy reaches the critical value.

This work was supported in part by RFBR (grant 13-02-00674) and by RAS Program “Quantum mesoscopic and disordered structures”. We are grateful to I.A. Fomin and G.E. Volovik for useful comments.

1. R.Sh. Askhadullin, P.N. Martynov, P.A. Yudintsev et al., J. Phys.: Conf. Ser. **98**, 072012 (2008).
2. K. Aoyama and R. Ikeda, Phys. Rev. **B**, **73**, 060504 (2006).
3. T. Kunimatsu, T. Sato, K. Izumina et al., Pis'ma v ZhETF **86**, 244 (2007) [JETP Lett. **86**, 216 (2007)].
4. V.V. Dmitriev, D.A. Krasnikhin, N. Mulders et al., Pis'ma v ZhETF **91**, 669 (2010) [JETP Lett. **91**, 599 (2010)].
5. J. Pollanen, J.I.A. Li, C.A. Collett, et al., Phys. Rev. Lett. **107**, 195301 (2011).
6. R.Sh. Askhadullin, V.V. Dmitriev, D.A. Krasnikhin, et al., Pis'ma v ZhETF **95**, 355 (2012) [JETP Lett. **95**, 326 (2012)].
7. V.V. Dmitriev, A.A. Senin, A.A. Soldatov et al., Zh. Exp. Teor. Fiz. **146**, #6(12) (2014, to be published) [JETP **119**, #6 (2014)].
8. G.E. Volovik, J. of Low Temp. Phys. **150**, 453 (2008).
9. J.A. Li, J. Pollanen, A.M. Zimmerman, et al., Nature Physics **9**, 775 (2013).
10. I.A. Fomin, J. of Low Temp. Phys. **31**, 509 (1978).
11. G.A. Baramidze, G.A. Kharadze, J. of Low Temp. Phys. **162**, 1 (2011).
12. D. Vollhardt, P. Wolfe, "The Superfluid Phases of  $^3\text{He}$ ", Taylor&Francis (1990).
13. V.P. Mineev, J. of Low Temp. Phys. **177**, 48 (2014).
14. G.A. Baramidze, G.A. Kharadze, Pis'ma v ZhETF **97**, 718 (2013) [JETP Lett. **97**, 621 (2013)].
15. B. Hanninen, E.V. Thuneberg, Phys. Rev. **B** **67**, 214507 (2003).
16. W.P. Halperin, H. Choi, J.P. Davis, J. Pollanen, J. of Phys. Soc. of Japan **77**, 111002 (2008).
17. E.V. Thuneberg, S.K. Yip, M. Fogelstrom, J.A. Sauls, Phys. Rev. Lett. **80**, 2861 (1998).
18. J.A. Li, A.M. Zimmerman, J. Pollanen et al., Phys. Rev. Lett. **112**, 115303 (2014).
19. J.A. Li, A.M. Zimmerman, J. Pollanen et al., J. of Low Temp. Phys. **175**, 31 (2014).
20. E.V. Surovtsev, Zh. Exp. Teor. Fiz. **135**, 705 (2009) [JETP **108**, 616 (2009)].
21. J.A. Sauls, Phys. Rev. **B**, **88**, 214503 (2013).